Available online at www.sciencedirect.com
ScienceDirect
Catalysis Today 128 (2007) 80–87
CATALYSIS TODAY
www.elsevier.com/locate/cattod

Novel supported Pd hydrogenation bionanocatalyst for hybrid homogeneous/heterogeneous catalysis

N.J. Creamer [a,*], I.P. Mikheenko [a], P. Yong [a], K. Deplanche [a], D. Sanyahumbi [a], J. Wood [b], K. Pollmann [c], M. Merroun [c], S. Selenska-Pobell [c], L.E. Macaskie [a]

[a] *School of Biosciences, University of Birmingham, Edgbaston, Birmingham B15 2TT, UK*
[b] *Department of Chemical Engineering, University of Birmingham, Edgbaston, Birmingham B15 2TT, UK*
[c] *Institute of Radiochemistry, FZD-Rossendorf, D-01314 Dresden, Germany*

Available online 18 June 2007

Abstract

Homogeneous and heterogeneous catalysis approaches to hydrogenation have different advantages and disadvantages and hybrid approaches are sought to maximise the advantages of both. Bacterial cells, of length 1–2 μm, present an economical alternative to conventional micro-scale supports such as graphite and alumina. Certain strains of bacteria can reduce soluble Pd(II), from stock solutions or acid extracts of spent catalysts, forming nanocrystals of Pd, which are supported within the bacterial cell surface layers. The biologically supported nano-Pd contains particles of size ~5 nm and below, as determined using magnetic measurements (SQUID) and EXAFS spectroscopy. Bio-nano-Pd supported on exemplar Gram negative and Gram positive bacterial types catalysed the hydrogenation of itaconic acid (initial rates 1.1 and 1.2×10^{-2} mol gPd^{-1} s^{-1}) comparing well with commercial 5% Pd-graphite (1.3×10^{-2} mol gPd^{-1} s^{-1}).
© 2007 Elsevier B.V. All rights reserved.

Keywords: *Bacillus sphaericus*; *Desulfovibrio desulfuricans*; Heterogeneous catalyst; Hydrogenation; Itaconic acid; Palladium

1. Introduction

In general, homogeneous catalysis is preferable to the heterogeneous approach due to higher chemical and energy utilisation efficiencies. This approach has been used extensively [1] but is precluded in those industrially important reactions, which employ expensive precious metal catalysts where metal retention is paramount. Attempts to overcome this difficulty have included ligand modification and the tethering of homogeneous catalyst on polymeric or inorganic supports in the liquid phase [2–4]. Heterogeneous catalysis is vitally important in organic syntheses and the production of fine chemicals [4–6] but in a mixed phase system the engineering challenges of mass transfer and mixing must be overcome for maximum product yield. Here, reactor design is critical, e.g. a cocurrent downflow bubble column reactor was developed to enhance mass transfer in slurry or fixed bed reactions [7,8].

Recently, nanoparticles have received intense attention because they demonstrate physical (and catalytic) properties that are different from those of bulk material [9,10]. Nanoparticulate palladium (Pd) has received particular attention because of the outstanding effectiveness of the metal as a catalyst, for e.g. hydrogenation and hydrogenolysis reactions [5,11]. However, preparation of metal nanoparticles involves rigorous experimental procedure or expensive equipment, or both [10,12,13]. This is in part due to the property of nanoparticles, which confers their high reactivity: a relatively high proportion of the atoms in a nanoparticle are present at its surface whereas in a larger particle the majority of atoms occupy the bulk. In nanoparticles, therefore, the influence of surface effects is significant compared to those of the particle bulk. One such effect is the promotion of particle growth [14], which occurs either by coalescence (the fusing of two or more smaller particles to form a larger one) or by ripening (the growth of large particles by migration of material from smaller ones). Accordingly, intervention is required to preserve the nanoparticles and maintain their particular physical properties for utilisation in the catalytic reaction of choice.

* Corresponding author. Tel.: +44 121 414 5434; fax: +44 121 414 5925.
E-mail address: n.j.creamer@bham.ac.uk (N.J. Creamer).

0920-5861/$ – see front matter © 2007 Elsevier B.V. All rights reserved.
doi:10.1016/j.cattod.2007.04.014

Palladium is a paramagnetic metal and the bulk metal is considered to be on the verge of ferromagnetism [15] while nanoscale Pd-clusters are ferromagnetic [16]. The onset of ferromagnetism can be invoked by the presence of a ferromagnetic impurity [17], expansion of the crystal lattice, a change in symmetry [18], the introduction of crystal defects [19], or the decreased coordination number of atoms at the surface of a crystal [18,20]. Ferromagnetism has been demonstrated in high purity palladium nanoparticles with radii of between 2 and 6 nm [21,22]. Nanoparticles of radii ∼1 nm are known not to show ferromagnetism, i.e. there is a lower limit [23].

For catalytic applications there are conflicting needs to maintain the nanoparticle format for high reactivity whilst satisfying the dual requirements for low mass transfer constraints and the need for catalyst recovery. The development of precious metal carbon-supported particles is an excellent compromise and commercial catalysts based on this formulation are available but expensive (palladium, US$ 352 per troy ounce metal, 26 March 2007) and can be used in, e.g. slurry reactors. An example fuel cell catalyst comprising a PtRu alloy on carbon black showed overall particle sizes of ∼50 nm with highly dispersed individual metallic nanoparticles of ∼1–5 nm on the carbon black support [24]. Such structures tend to clump [24], leading to segregation of the solid and liquid phase. This behaviour is of particular importance as it leads to a substantial increase in the effective particle size resulting in a decreased conversion rate [25]. A cocurrent three-phase downflow bubble column reactor (CDC) was found particularly useful using an example model reaction, hydrogenation of itaconic acid (Eq. (1)) [8]:

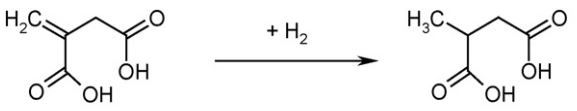

itaconic acid methyl succinic acid (1)

This system employed a commercial catalyst (Pd type 37; Johnson–Matthey; 5% and 10% Pd on charcoal; metal areas were 13.9 and 35.9 $m^2\ g^{-1}$ catalyst). The overall efficiency was dependent on both the gas–liquid and liquid–solid mass transfers [8].

Recently, the use of bacteria as precious metal nanocatalyst supports has received attention. Bacterial cells, typically in the size range of 1–5 μm (i.e. ∼1000-fold larger than the ferromagnetic Pd-clusters and up to 100-fold larger than carbon-supported particles: see above) have the advantage of easy use in suspension but are sufficiently heavy when metallized to fall under gravity. If required, bacterial catalysts can be easily used in a two-phase system by utilising the ability of bacteria to form self-adhesive biofilms on solid mesh or particulate supports before metallization [26] for use in conventional flow-through [27,28] or fluidised bed systems. The biofilm surface itself is typically highly convoluted [29], which gives scope for a far greater surface area than that imparted by the support material alone, effectively amplifying the catalyst support area.

The use of bacterial cells as carriers for precious metal nanoparticles is a major step-change in catalysis. The exemplar system is the sulfate-reducing bacterium *Desulfovibrio desulfuricans* [30], which reduces soluble Pd(II) to Pd(0). Palladized cells had a high catalytic activity in test reactions involving the production of hydrogen from hypophosphite [31], the hydrogenolytic dehalogenation of polychlorinated biphenyls [32] and the reduction of Cr(VI) to Cr(III) in batch suspension [33] or flow-through reactor [34,35] systems. It was recently shown that catalytically effective Bio-Pd-catalyst could even be biomanufactured from industrial wastes and scrap [35], further increasing the potential for an alternative economic strategy for industrial catalyst production.

The mechanism of Bio-Pd manufacture in *D. desulfuricans* is quite well understood. Initially, incoming soluble Pd(II) coordinates to oxygen and amine groups [36], which are on or near a hydrogenase enzyme which mediates the reduction of Pd(II) to Pd(0) via oxidation of H_2. Mutants deleted with respect to specific hydrogenases relocated their Pd deposits to the site of the activity of the remaining hydrogenase(s) [37], confirming the involvement of this enzyme in Pd-cluster formation. Following nucleation of Pd(0) further cluster growth then occurs to make cell-bound deposits of catalytically active Pd-nanoparticles stabilised by the architecture of the bacterial matrix.

Bacterial cells fall into two fundamentally different types categorised by their response to a diagnostic staining reaction (the Gram strain), which reflects the binding of a dye to characteristic cell wall polymers [38] to give, respectively, Gram positive and Gram negative types. *D. desulfuricans* is a typical Gram negative cell, the cell envelope of which is a double membrane structure comprising the cytoplasmic membrane and an outer membrane, between which is a 'compartment' (the periplasmic space) comprising a matrix of carbohydrate-based polymers and proteins [39] including hydrogenases [37]. The outer membrane is permeable to atoms and small molecules and, accordingly, deposition of Pd occurs within the periplasmic space and also on the inner membrane, corresponding to the locations of the three major hydrogenases of this species [37].

In contrast, the Gram positive cell envelope [40,41] comprises only a cytoplasmic membrane and a thick peptidoglycan layer but no outer membrane. It also contains specific polymers (teichoic and lipoteichoic acids) and a periplasmic space, once conjectural [41] but now confirmed [42,43]. The *Bacillus sphaericus* strain studied here is additionally covered by a highly ordered proteinaceous surface layer (S-layer) [44].

Since the above suggests that *D. desulfuricans* and *B. sphaericus* may deposit Pd by fundamentally different mechanisms involving very different biochemical support matrices, the first objective of this study was to compare the biofabrication of Pd catalyst by the two strains. The second objective was to compare the catalytic efficacy of the respective Bio-$Pd_{D.\ desulfuricans}$ and Bio-$Pd_{B.\ sphaericus}$ in the model reaction, hydrogenation of itaconic acid, as compared to a commercial catalyst, in a stirred batch reactor. We discuss the

results obtained with respect to the nanoparticle location by using TEM, and the size of the respective two Bio-Pds determined magnetically and by the use of extended X-ray absorption fine structure (EXAFS) spectroscopy.

2. Materials and methods

2.1. Bacterial strains and growth conditions

D. desulfuricans ATCC 29577 was grown anaerobically in Postgate's medium C, harvested by centrifugation and processed as described previously [30]. *B. sphaericus* JG-A12 was isolated from a soil sample collected from the uranium mining waste pile 'Haberland' near Johanngeorgenstadt, Germany [45]. The *B. sphaericus* cells were routinely grown aerobically with shaking in nutrient broth (NB) medium consisting of 5 g l^{-1} peptone and 3 g l^{-1} meat extract.

2.2. Metallization of bacteria

Bio-supported palladium particles were prepared by reduction of sodium tetrachloropalladate(II) onto *D. desulfuricans* using hydrogen gas as the electron donor [30]. Palladization of *B. sphaericus* was carried out using the same method. The mass ratio of Pd(II) in solution to the dry weight of cells was adjusted depending on mass percent loading required. The Pd loaded bacterial cells were centrifuged and washed three times with distilled water and once with acetone then dried in air.

2.3. Electron microscopy

Pellets of freshly harvested Pd-loaded bacteria were fixed in 2.5% (w/v) aqueous glutaraldehyde, centrifuged, re-suspended in 1.5 ml of 0.1 M cacodylate buffer (pH 7.0) and stained in 1% osmium tetroxide in 0.1 M phosphate buffer, pH 7.0 (60 min) for transmission electron microscopy (TEM). Samples were dehydrated using an ethanol series. After two 15 min washes in propylene oxide cells were embedded in epoxy resin. Sections (90–100 nm thick) were cut from the resin block, placed onto a copper grid and viewed with a JEOL 120CX2 transmission electron microscope (TEM); accelerating voltage 80 kV.

2.4. Solid state analysis

Magnetic measurements. The magnetic properties of Bio-$Pd_{D.\ desulfuricans}$ and Bio-$Pd_{B.\ sphaericus}$ and their chemically prepared counterpart ('Chem-Pd': Pd(II) reduced to Pd(0) under H_2) were investigated using a vibrating sample magnetometer VSM (Oxford Instruments, UK) and a superconducting quantum interference device (SQUID: Quantum Design, USA). The temperature range was 10–300 K and applied magnetic fields were from 0.0005 T to 2 T; usually 1–2 T unless stated otherwise. All measurements are expressed per gram of palladium and accuracy is limited by mass determination to ±10%. The main difficulty encountered in carrying out measurements in a field of this strength is the presence of a background diamagnetic moment from the sample holder and the polymer film used to contain the Bio-Pd powder. A methodology was developed to minimize this [46] and it was adopted here.

XAS measurements. Palladium K-edge X-ray absorption spectra were collected at the Rossendorf Beamline (ROBL) located at the European Synchrotron Radiation Facility (ESRF), Grenoble (France) [47] using a Si(1 1 1) double-crystal monochromator and Si-coated mirrors for focusing and rejection of higher harmonics. Samples were cooled to 30 K in a closed-cycle He cryostat, and data were collected in transmission mode using an Ar flushed ionisation chamber. The energy was calibrated by measuring the Pd K-edge transmission spectrum of a palladium foil and defining the first inflection point as 24,350 eV. The Pd-loaded sample was measured as dry sample. The EXAFS oscillations were isolated from the raw, averaged data by removal of the pre-edge background, approximated by a first-order polynomial, followed by μ_0-removal via spline fitting techniques and normalization using a Victoreen function. The amplitude reduction factor was held constant at 1.0 for the FEFF8 calculation and EXAFS fits. The shift in threshold energy, ΔE_0, was varied as a global parameter in the fits. The theoretical scattering phase and amplitude functions used in data analysis were calculated using X-ray data from Pd foil using the FEFF8 program [48].

2.5. Determination of catalytic activity of Bio-$Pd_{D.\ desulfuricans}$ and Bio-$Pd_{B.\ sphaericus}$

Bio-Pd (5%, (w/w) or as stated (total weight of palladium used was 5 mg) or Chem-Pd (reference sample; equivalent mass as Pd) was added to 250 ml itaconic acid solution (50 mg l^{-1} approx.) in a High Pressure Stainless Steel Autoclave Reactor (500 ml: Baskerville). The reactor was purged with hydrogen (10 min) then held under hydrogen (5 atm.) and heated to 70 °C. The reaction mixture was stirred at 1000 rpm when the reaction temperature had been attained, with the reaction time measured from this point. Withdrawn samples were analysed using a VECTOR 33 FT-IR spectrometer (Bruker Optics) configured for near-infrared operation using a tungsten halogen NIR source, a thermoelectrically cooled InAs detector sensitive over the range of 12,800–3470 cm^{-1} and a NIR quartz beam splitter. A fibre optic dip probe was used to carry out the NIR measurements. Spectrometer measurements were carried out using Bruker OPUS/IR software. Quantitative analysis of FT-IR spectra was carried out as described by Wood and Turner [49].

3. Results and discussion

3.1. Deposition of Pd by D. desulfuricans and B. sphaericus

Bacteria examined before palladization were grey and indistinct with the contrast (grey areas) attributed to the osmium stain (Fig. 1A and B). After palladization under H_2 (5%, w/w) both types of cells were surrounded by an electron-opaque layer

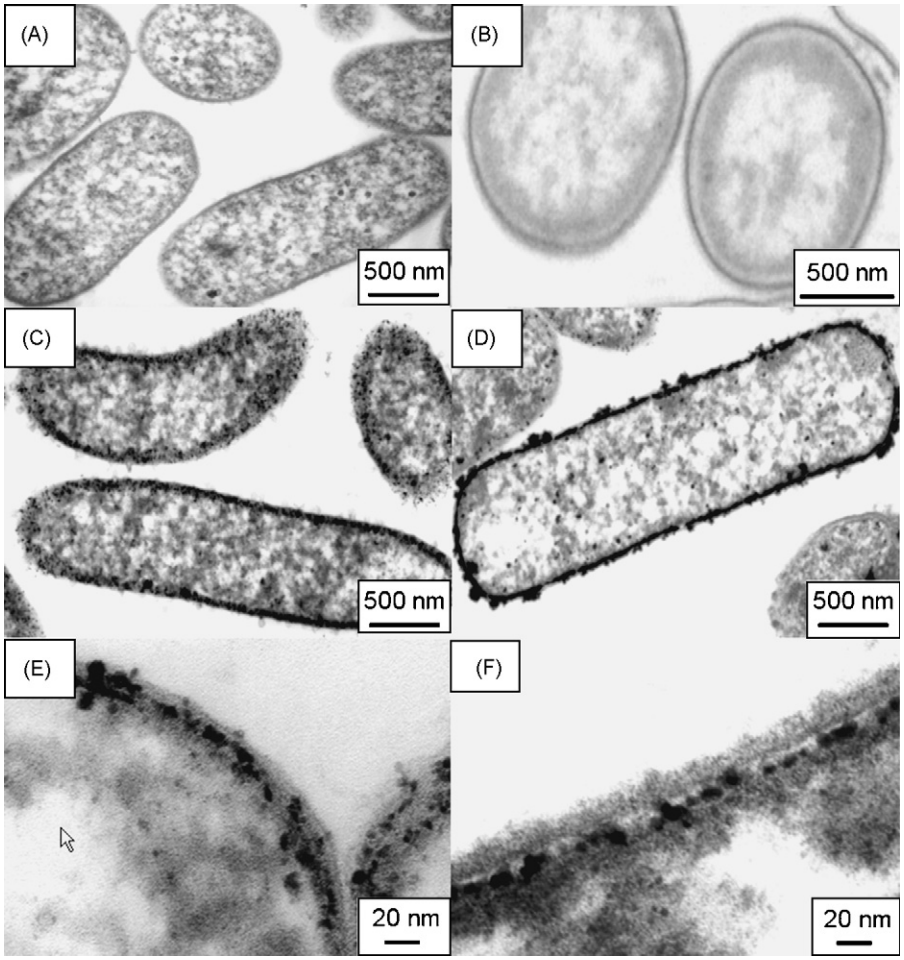

Fig. 1. Deposition of Pd by *Desulfovibrio desulfuricans* (A, C and E) and *Bacillus sphaericus* (B, D and F). (A and B) Cells before palladization. (C and D) Cells palladized to 5% of the dry weight. (E and F) Expanded area of cell surfaces to show Pd-nanoparticles. (B) is from archive material at FZD-Rossendorf. *Note*: these cells are cut transversely and hence appear round.

at the cell periphery (Fig. 1C and D), resolvable to individual particles (Fig. 1E and F) which were shown previously to comprise palladium by energy dispersive X-ray microanalysis, with the crystalline nature of the material shown by the sharp nature of the X-ray powder pattern which confirmed the speciation as Pd(0) with $Pd_{D.\ desulfuricans}$ [46]. Similar tests in this study using the Bio-$Pd_{B.\ sphaericus}$ gave identical results (not shown). High-resolution electron micrographs (Fig. 1E and F) show that Pd was held as discrete nanoparticles beneath the outermost layers of the cells within the periplasmic space bounded by the Gram negative double membrane structure (*D. desulfuricans*: Fig. 1E) or between the peptidoglycan and the S-layer of the Gram positive *B. sphaericus* (Fig. 1F). In each case the palladium nanoparticles were held enclosed beneath the outer most cell layers (Fig. 1E and F). Although the Pd-particles appeared to be distinct by visual examination (Fig. 1) the polymeric nature of the intertwined cell surface layers (phospholipids, proteins, carbohydrates, peptidoglycan and teichoic/lipoteichoic acids, the latter being specific to Gram positive cells: see Section 1) means that there are many biochemical candidates to support the growing Pd-clusters and hold them as stable entities. Single molecule width inter-particle distances are below the resolution of the electron microscope, therefore physical methods were employed to estimate the nanoparticle sizes of the Pd-cluster populations.

3.2. Determination of nanoparticle sizes by solid-state analysis

A combination of a linear and non-linear magnetic behaviour was recorded for Bio-$Pd_{D.\ desulfuricans}$ and Bio-$Pd_{B.\ sphaericus}$ samples in response to varying external magnetic field (H). In common with other authors we associate the linear dependence of magnetisation on the applied external field strength (m/H) with paramagnetism and the non-linear dependence with a form of ferromagnetic behaviour [50]. For each sample, the ferromagnetic component of the magnetic moment was derived by subtracting the linear component. Fig. 2 shows the net ferromagnetic component for both samples at room temperature. The moments shown are per gram of Pd, which is 5% of the total sample mass.

In order to estimate the size of the ferromagnetic particles it is necessary to fit the ferromagnetic component of the samples using the Langevin function [15]. This yields the quantity μ, the magnetic moment per magnetic particle. A typical value obtained is 215 μ_B. From this, and knowing that the spacing

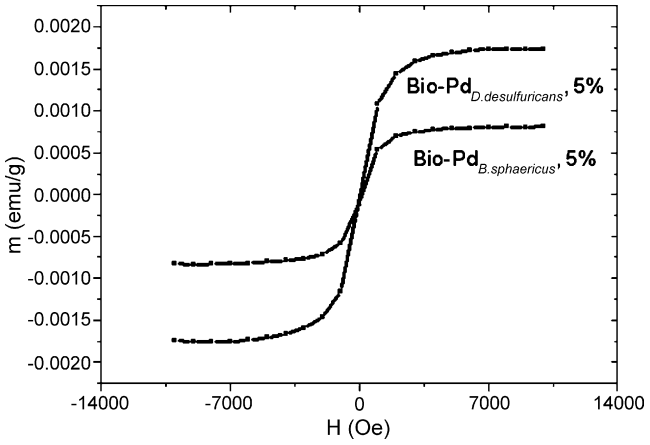

Fig. 2. Non-linear component of magnetic moment as a function of the applied magnetic field for Bio-Pd$_{D.\ desulfuricans}$ and $_{B.\ sphaericus}$ (5% loading by mass).

between the Pd atoms in a cubic close-packed crystal is 0.388 nm, it is possible to calculate the size of the particle. There is still no agreement as to whether the ferromagnetism of palladium nanoparticles resides in all the constituent atoms equally or only in the surface atoms [16] so we carried out the calculation using both models. Assuming that all the atoms in a cubic particle have an equal magnetic moment of 0.12 μ_B per atom [21], the particle would comprise approximately 1800 atoms and would measure 4.7 nm along each edge. In the second model, where the magnetic moment of each surface palladium atom is assumed to be 0.23 μ_B per atom [18], the particle would have 934 surface atoms and measure 4.8 nm along each edge. Both of these estimates are consistent with the findings of Taniyama et al. [21] and Cox et al. [23].

These interpretations hold for a pure Pd sample and assume that there is no contamination with Fe, a component of biological materials including hydrogenase enzymes. Since the incoming Pd(II) coordinates to amine groups and these are deduced to be on or near the hydrogenase enzymes (see above) it is essential to discount a contribution by Fe. Element-specific magnetism is determined by the use of X-ray magnetic circular dichroism (XMCD). Analysis of Bio-Pd$_{D.\ desulfuricans}$ using XMCD at ESRF Grenoble confirmed that the magnetic effect was palladium-specific (I.P. Mikheenko and P.M. Mikheenko, unpublished). These studies will be reported in full in a later publication. Importantly, they validate the use of conventional calculation methods to obtain the nanoparticle size, based on magnetic measurements.

As an alternative, EXAFS spectroscopy has been used in this work to study the radial distribution of the nearest neighbours as well as to determine the size of the Pd nanoparticles. EXAFS spectroscopy has become a widespread method for determining particle diameter in highly dispersed metals. Conventional transmission electron microscopy (TEM) allows the detection of metal particles of 1.5–2.0 nm in diameter but TEM does not provide average values, only information about each particle. Moreover, very small metal particles can be damaged by the electron beam. Also, the low limit of metal particle detection does not allow study of the metallic phase of highly dispersed samples [51]. In the presence of a distribution of different particle sizes, EXAFS gives a mean dimension weighted by the fraction of atoms of different sizes [52]. This technique was used successfully to determine the size of gold nanoparticles formed on the cells and S-layer sheets of *B. sphaericus* JG-A12 [53] and of Pd nanoclusters formed on immobilized cells of this bacterium [54].

Fig. 3 shows the Pd K-edge EXAFS spectra of a palladium foil and of Pd-loaded cells along with their corresponding Fourier transform (FT). The fit parameters of the calculated spectra are given in Table 1. The signal to noise ratio is excellent, which makes data analysis possible to a wave vector

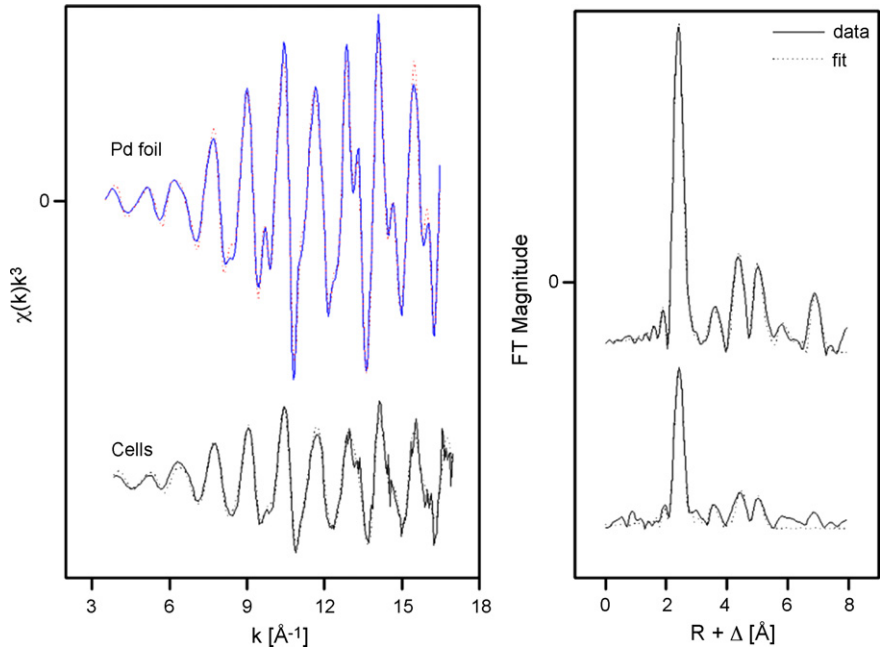

Fig. 3. EXAFS spectra of Pd foil and Pd-loaded cells of *B. sphaericus* JG-A12 and their corresponding FT.

Table 1
EXAFS structural parameters of the palladium foil and Pd-loaded cells

Sample	Shell	N[a]	R (Å)[b]	σ^2 (Å^2)[c]	ΔE (eV)
Pd foil	Pd–Pd_1	11.5 ± 0.4	2.75	0.0021	−18.0
	Pd–Pd_2	4.2 ± 0.9	3.89	0.0019	
	Pd–Pd_3	17.6 ± 2.0	4.77	0.0026	
	Pd–Pd_4	14.0 ± 2.0	5.41	0.0013	
Cells	Pd–Pd_1	6.5 ± 0.5	2.75	0.0028	−13.0
	Pd–Pd_2	1.7 ± 0.7	3.90	0.0021	
	Pd–Pd_3	6.1 ± 1.0	4.78	0.0025	
	Pd–Pd_4	6.7 ± 1.3	5.41	0.0025	

[a] Errors in coordination numbers are ±25% and standard deviations as estimated by EXAFSPAK.
[b] Errors in distance are ±0.02 Å.
[c] Debye–Waller factor.

k of 17 Å^{-1}. It is well established that the FT of $\chi(k)$ over a finite k range is a radial structure function exhibiting a series of peaks whose positions and magnitudes are related to the interatomic distances and the number of atoms in the different coordination shells, respectively. FT peak distances R are reported in units of Å and are uncorrected for scattering phase shift, i.e. $R + \Delta R$.

In the case of the Pd foil sample, the FT peaks of metallic Pd were attributed to four Pd–Pd shells with distances of 2.75, 3.89, 4.77 and 5.41 Å. The major peak corresponds to about 12 Pd atoms at a Pd–Pd interatomic distance of 2.75 ± 0.01 Å as reported by Polizzi et al. [52] and in agreement with X-ray diffraction studies.

The EXAFS spectrum obtained for the Pd/cell sample is very similar to the spectrum of Pd foil. Four distinct peaks at 2.75, 3.90, 4.78 and 5.41 Å each corresponding to Pd atoms was found in the FT of the experimental spectrum. The coordination numbers (N) of the different Pd–Pd bond distances of this sample are different from the bulk ones, showing the presence of small metal particles. The reduction of the coordination numbers was used to estimate the average size of the studied sample assuming a spherical shape. The palladium–palladium first shell coordination number of 6.5 ± 0.5 as found for the Bio-$Pd_{B.\ sphaericus}$ analyzed in this study corresponds to metal particles that fit just inside S-layer protein pores of the cells of *B. sphaericus* JG-A12. Assuming spherical metal particles with FCC lattice, the average cluster size was calculated [55]. A mean Pd–Pd coordination number 6–7 corresponds to an average particle diameter between 0.8 and 1 nm. The discrepancy in the size of the Pd-nanoparticles formed by *B. sphaericus* JG-A12, measured by SQUID and EXAFS spectroscopy found in this work has also been described for other systems using different techniques. Polizzi et al. [52] reported that the size of Pd-nanoparticles in the Pd/SiO_2 system given by EXAFS data analysis was smaller than that found using ASAXS and WAXS techniques. They speculate that in the presence of a distribution of different particle sizes, EXAFS gives a mean dimension weighted by the fraction of atoms corresponding to the different sizes. In the sample studied, as shown by ASAXS and partially by WAXS, the majority of Pd atoms is in the smaller particles.

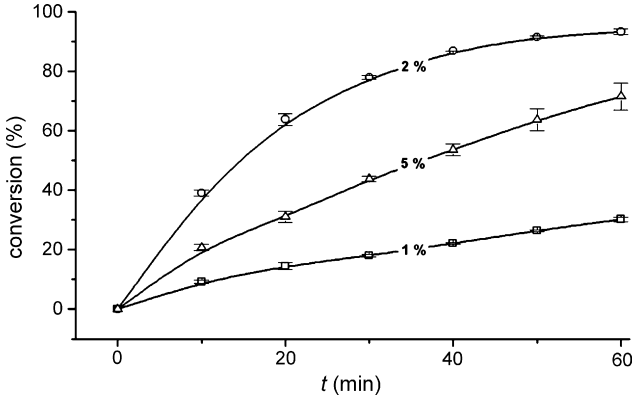

Fig. 4. Percentage conversion of itaconic acid using three preparations of palladium (1%, 2% and 5% by mass) supported on *B. sphaericus*. Values are averages of three or more experiments and error bars represent the standard error of the mean. Where error bars are not shown these are within the dimensions of the symbols.

This explains why the larger ones are not revealed by EXAFS [52].

3.3. Catalytic activity of Bio-$Pd_{D.\ desulfuricans}$ and Bio-$Pd_{B.\ sphaericus}$

It is concluded from the physical studies above that the biomaterials contained Pd-nanoparticles of sizes of between ~1–6 nm and hence a high catalytic activity would be expected, assuming that the outermost cell layers of the bacteria studied do not pose a significant barrier to substrate access. The hydrogenation of itaconic acid was chosen as a test reaction since this is a well-defined model hydrogenation system, which has been shown scalable to reactor types suitable for commercial applications (see Section 1). Previous studies using the reduction of Cr(VI) to Cr(III) as a criterion of catalytic activity of Bio-$Pd_{D.\ desulfuricans}$ showed that a loading of 1:19 (5% Pd on biomass) was optimal [56] and this was adopted for the current study, in comparison with a commercial 5% Pd on carbon catalyst.

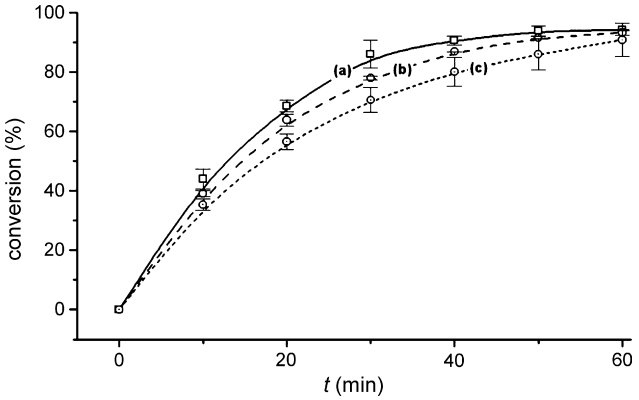

Fig. 5. Percentage conversion of itaconic acid using three preparations of supported palladium. (a) 5% on graphite (Johnson–Matthey), (b) 2% on *B. sphaericus* and (c) 5% on *D. desulfuricans*. Data are means ± S.E.M. Where error bars are not shown these are within the dimensions of the symbols.

Table 2
Initial rates of conversion of itaconic acid by five catalysts (averaged over 10 min)

Catalyst	Initial rate ($\times 10^{-3}$ mol gPd^{-1} s^{-1})
Pd-graphite 5% (JM)	13.0
$Pd_{D.\ desulfuricans}$ 5%	11.0
$Pd_{B.\ sphaericus}$ 5%	6.1
$Pd_{B.\ sphaericus}$ 2%	12.0
$Pd_{B.\ sphaericus}$ 1%	2.2

A comparison of Bio-$Pd_{B.\ sphaericus}$ loaded with Pd at 1%, 2% and 5% shows the percentage conversion of itaconic acid as a function of time for three preparations of palladium supported on *B. sphaericus*. In all cases the reaction curves follow first order behaviour in terms of itaconic acid concentration. There is a clear difference in the initial rate of the reaction and in the total conversion of itaconic acid when the reaction was stopped after 60 min. The initial rate achieved by the 2% loaded sample is greater than that observed with the 1% (Fig. 4). This is consistent with what would be expected from either a larger number of particles of similar size or a similar number of larger particles. In either case the total surface area of the catalyst would be increased resulting in a higher turnover and therefore a higher reaction rate. The behaviour of the 5% loaded sample is at variance with this expectation and the rate achieved in this case is lower than that of the 2% sample. This may be attributable to the finite number of nucleation loci on the bacterial surface. Recent work with purified *B. sphaericus* S-layer material has identified pockets containing stretches of carboxylated amino acids [57,58] associated with metal particle formation. The pockets have been shown to separate the individual nanoparticles and prevent coalescence whilst allowing them to grow to a maximum diameter determined by the size of the pockets. As long as the amount of metal present is not sufficient to fill the total space in the S-layer pockets the nanoparticles remain discreet. However, a metal loading beyond this maximum would lead to growth beyond the size limit causing metal particles to overflow the pockets and contact one another. For this reason, in this case increased loading does not lead to the formation of more particles but rather a lower number of larger particles, probably with lower overall catalytic activity.

Fig. 5 compares the conversion of itaconic acid by the commercial catalyst (5% palladium on graphite) with that achieved using preparations of the two biologically supported catalysts: 2% Pd on *B. sphaericus* and 5% Pd on *D. desulfuricans*. The initial rates for all five catalysts are summarised in Table 2. For the 2% *B. sphaericus* catalyst the value was 92% compared to the commercial catalyst and for the 5% *D. desulfuricans* preparation it was 85%. Values for total conversion after 60 min were 99% and 97%, respectively, of that achieved using the commercial catalyst.

4. Conclusions

This study shows that by using bacterial cells as support materials for Pd-nanoparticles, with simple biomanufacture from Pd(II) solution under H_2, it is possible to make a hybrid homogeneous/heterogeneous catalyst which is as effective catalytically as commercial 5% Pd on graphite, for which good separation of catalyst and product remains problematic. The reaction rate and extent of conversion were comparable for both the Gram positive and Gram negative cells as well as the commercial material. Since the Pd-nanoparticles are held below the outermost bacterial surface layers it might be expected that mass transfer limitations through these peripheral layers could apply. In this case the reaction rate could be potentially higher than with current commercial materials; it must be emphasised that the biomasses were not treated in any way. Hence, post-harvest processing might prove additionally beneficial and this will form a focus of future work as will investigations into the possible selectivity of biologically supported palladium catalysts. The role of hydrogenase is well established in *D. desulfuricans* but such a role is unlikely for *B. sphaericus* under the conditions studied and an alternative mechanism of Pd(II) reduction is possible. Various other bacterial enzymes, well documented elsewhere to have 'metal reductase' activity, could expand the potential portfolio of biomolecular candidates for metallic nanoparticle biomanufacture.

Acknowledgements

This study was supported by EC contract GRD1-2001-40424 and the EPSRC and BBSRC (grant nos. EP/D05768X/1, BB/C516128/1 and BB/E003788/1). We thank A.C. Scheinost, A. Rossberg, C. Hennig, and H. Funke (ROBL, Grenoble) for their help in EXAFS measurements. We also thank Dr. P.M. Mikheenko for invaluable help with magnetic analysis and interpretation of magnetic data.

References

[1] B. Cornils, W.A. Herrmann, Applied Homogeneous Catalysis with Organometallic Compounds: A Comprehensive Handbook, VCH, Weinheim, Germany, 1996.
[2] J.M. Thomas, W.J. Thomas, Principles and Practice of Heterogeneous Catalysis, VCH, Weinheim, Germany, 1997.
[3] V.M. Frolov, Plat. Met. Rev. 40 (1996) 8–18.
[4] J.H. Clark, D.J. Macquarrie, Heterogeneous catalysis in liquid phase transformations of importance in the industrial preparation of fine chemicals, Org. Proc. Rev. Dev. 1 (1997) 149–162.
[5] S. Nishimura, Handbook of Heterogeneous Catalytic Hydrogenation for Organic Syntheses, John Wiley & Sons, New York, USA, 2001.
[6] A. Tungler, T. Tarnai, L. Hegedûs, K. Fodor, T. Máthé, Plat. Met. Rev. 42 (1998) 108–115.
[7] A.P. Boyes, A. Chughtai, X.X. Lu, S. Raymahasay, S. Sarmento, M.W. Tilston, J.M. Winterbottom, Chem. Eng. Sci. 47 (1992) 3729–3796.
[8] X.X. Lu, A.P. Boyes, J.M. Winterbottom, Chem. Eng. Sci. 51 (1996) 2715–2720.
[9] W. Eberhardt, Surf. Sci. 500 (2002) 242–270.
[10] H. Hori, T. Teranishi, Y. Nakae, Y. Seino, M. Miyake, S. Yamada, Phys. Lett. A 263 (1999) 405–410.
[11] C. Schuth, M. Reinhard, Appl. Catal. B: Environ. 18 (1998) 215–221.
[12] P. Mulvaney, L.M. Liz-Marzan, M. Giersig, T. Ung, J. Mater. Chem. 10 (2000) 1259–1270.
[13] T. Taniyama, T. Sato, E. Ohta, M. Takeda, Physica B 213 (1995) 254–256.
[14] T.V. Choudhary, D.W. Goodman, Top. Catal. 21 (2002) 25–34.

[15] S.V. Vonsovskii, Magnetism, Wiley, New York, 1974.
[16] T. Taniyama, E. Ohta, T. Sato, Physica B 237 (1997) 286–288.
[17] T. Shinohara, T. Sato, T. Taniyama, I. Nakatani, J. Magn. Magn. Mater. 197 (1999) 94–95.
[18] L. Vitos, B. Johansson, J. Kollar, Phys. Rev. B 62 (2000) R11957–R11960.
[19] N. Takano, T. Kai, K. Shiiki, F. Terasaki, Solid State Commun. 97 (1996) 153–156.
[20] A.E. Garcia, V. Gonzalez-Robles, R. Baquero, Phys. Rev. B 59 (1999) 9392–9401.
[21] T. Taniyama, E. Ohta, T. Sato, Europhys. Lett. 38 (1997) 195–200.
[22] D. Mendoza, F. Morales, R. Escudo, J. Walter, J. Phys. Condens. Matt. 11 (1999) L317–L322.
[23] A.J. Cox, J.G. Louderback, S.E. Apsel, L.A. Bloomfield, Phys. Rev. B 49 (1994) 12295–12298.
[24] T.R. Ralph, M.P. Hogarth, Plat. Met. Rev. 46 (2002) 117–135.
[25] M. van der Zon, P.J. Hamersma, E.K. Poels, et al. Catal. Today 48 (1999) 131–138.
[26] L.E. Macaskie, P. Yong, M. Paterson-Beedle, A.C. Thackray, P.M. Marquis, R.L. Sammons, K.P. Nott, L.D. Hall, J. Biotechnol. 118 (2005) 187–200.
[27] M. Paterson-Beedle, K.P. Nott, L.E. Macaskie, L.D. Hall, Meth. Enzymol. 337 (2001) 285–305.
[28] L.E. Macaskie, R.M. Empson, F. Lin, M.R. Tolley, J. Chem. Technol. Biotechnol. 63 (1995) 1–16.
[29] V.J.M. Allan, M.E. Callow, L.E. Macaskie, M. Paterson-Beedle, Microbiology 148 (2002) 277–288.
[30] J.R. Lloyd, P. Yong, L.E. Macaskie, Appl. Environ. Microbiol. 64 (1998) 4608–4609.
[31] P. Yong, N.A. Rowson, J.P.G. Farr, I.R. Harris, L.E. Macaskie, Biotechnol. Bioeng. 80 (2002) 369–379.
[32] V.S. Baxter-Plant, I.P. Mikheenko, L.E. Macaskie, Biodegradation 14 (2003) 83–90.
[33] A.N. Mabbett, P. Yong, J.P.G. Farr, L.E. Macaskie, Biotechnol. Bioeng. 87 (2004) 104–109.
[34] A.C. Humphries, K.P. Nott, L.D. Hall, L.E. Macaskie, Biotechnol. Bioeng. 90 (2005) 589–596.
[35] A.N. Mabbett, D. Sanyahumbi, P. Yong, L.E. Macaskie, Environ. Sci. Technol. 40 (2006) 1015–1021.
[36] I. de Vargas, D. Sanyahumbi, M.A. Ashworth, C.M. Hardy, L.E. Macaskie, in: S.T.L. Harrison, D.E. Rawlings, J. Petersen (Eds.), Proceedings of the 16th International Biohydrometallurgy Symposium, Cape Town, South Africa, Published by 16th International Biohydrometallurgy Symposium, Cape Town, 2005, , pp. 605–616, ISBN 1-920051-17-1.
[37] I.P. Mikheenko, P.M. Mikheenko, S. Dementin, M. Rousset, L.E. Macaskie, in: S.T.L. Harrison, D.E. Rawlings, J. Petersen (Eds.), Proceedings of the 16th International Biohydrometallurgy Symposium, Cape Town, South Africa, Published by 16th International Biohydrometallurgy Symposium, Cape Town, 2005, , pp. 383–387, ISBN 1-920051-17-1.
[38] T.J. Beveridge, L.L. Graham, Microbiol. Rev. 55 (1991) 684–705.
[39] T.J. Beveridge, J. Bacteriol. 101 (1999) 4725–4733.
[40] T.J. Beveridge, V.R.F. Matias, in: V.A. Fischetti, R.P. Novick, J.J. Ferrati, D.A. Portnoy, J.I. Rood (Eds.), Ultrastructure of the Gram Positive Cell Walls in Gram Positive Pathogens, 2nd ed., ASM Press, Washington, USA, 2006.
[41] W.W. Navarre, O. Schneewind, Microbiol. Mol. Biol. Rev. 63 (1999) 174–229.
[42] V.R.F. Matias, T.J. Beveridge, Mol. Microbiol. 56 (2005) 240–251.
[43] V.R.F. Matias, T.J. Beveridge, J. Bacteriol. 188 (2006) 1011–1021.
[44] K. Pollmann, J. Raff, M. Schnorpfeil, G. Radeva, S. Selenska-Pobell, Microbiology 151 (2005) 2961–2973.
[45] S. Selenska-Pobell, P. Panak, V. Miteva, I. Boudakov, G. Bernhard, H. Nitsche, FEMS Microbiol. Ecol. 29 (1999) 59–67.
[46] I.P. Mikheenko, Ph.D. thesis, The University of Birmingham, UK, 2004.
[47] W. Matz, N. Schell, G. Bernhard, F. Prokert, T. Reich, J. Claußner, W. Oehme, R. Schlenk, S. Dienel, H. Funke, F. Eichhorn, M. Betzel, D. Pröhl, U. Strauch, G. Hüttig, H. Krug, Neumann, V. Brendler, P. Reichel, M.A. Denecke, H. Nitsche, J. Synchrotron Radiat. 6 (1999) 1076–1085.
[48] A.L. Ankudinov, B. Ravel, J.J. Rehr, S.D. Conradson, Phys. Rev. B 58 (1998) 7565–7575.
[49] J. Wood, P.H. Turner, Appl. Spectrosc. 57 (2003) 293–298.
[50] I.P. Mikheenko, P.M. Mikheenko, C.N.W. Darlington, C.M. Muirhead, L.E. Macaskie, in: V.S.T. Ciminelli, O. Garcia, Jr. (Eds.), Magnetic Testing of Pd Loaded Bacteria. Biohydrometallurgy: Fundamentals, Technology and Sustainable Development. Part B. Biosorption and Bioremediation, Elsevier, Amsterdam, 2001, pp. 681–688.
[51] D.C. Díaz-Moreno, A. Koningsberger, A. Munoz-Páez, Nucl. Instrum. Meth. B 33 (1997) 15–23.
[52] S. Polizzi, P. Riello, A. Balerma, A. Benedetti, Phys. Chem. 3 (2001) 4614–4619.
[53] M. Merroun, A. Rossberg, C. Hennig, A. Scheinost, S. Selenska-Pobell, Mater. Sci. Eng. C 27 (2007) 188–192.
[54] K. Pollmann, M.L. Merroun, J. Raff, C. Hennig, S. Selenska-Pobell, Lett. Appl. Microbiol. 43 (2006) 39–45.
[55] E.H. Voogt, Numie Software, Debye Institute, Utrecht University, Utrecht, The Netherlands, 1996.
[56] I.P. Mikheenko, K. Deplanche, P. Yong, N.J. Creamer, J. Wood, L.E. Macaskie, Environ. Appl. Microbiol., submitted for publication.
[57] R. Wahl, M. Mertig, J. Raff, S. Selenska-Pobell, W. Pompe, Adv. Mater. 13 (2001) 736–740.
[58] K. Fahmy, M. Merroun, J. Raff, K. Pollmann, Ch. Hennig, O. Savchuk, S. Selenska-Pobell, J. Biophys. 91 (2006) 996–1007.